Inhibition of Cav3.2 T-type Calcium Channels by Its Intracellular I-II Loop

Arnaud Monteil, Patrick Chausson, Katia Boutourlinsky, Alexandre Mezghrani, Iulia Blesneac, Isabelle Bidaud, Sylvaine Huc-Brandt, Céline Lemmers, Nathalie Leresche, Régis C Lambert, et al.

THE JOURNAL OF BIOLOGICAL CHEMISTRY VOL. 290, NO. 26, pp. 16168–16176, June 26, 2015

Inhibition of Cav3.2 T-type Calcium Channels by Its Intracellular I-II Loop*

Received for publication, December 19, 2014, and in revised form, April 30, 2015 Published, JBC Papers in Press, April 30, 2015, DOI 10.1074/jbc.M114.634261

Arnaud Monteil[‡§¶‖], Patrick Chausson[‡‡§§], Katia Boutourlinsky[**‡‡§§], Alexandre Mezghrani[‡§‖], Sylvaine Huc-Brandt[‡§‖], Iulia Blesneac[‡§‖], Isabelle Bidaud[‡§‖], Céline Lemmers[‡§¶‖], Nathalie Leresche[**‡‡§§], Régis C. Lambert[**‡‡§§], and Philippe Lory[‡§‖1]**

From the [‡]Université de Montpellier, CNRS UMR 5203, Département de Physiologie, Institut de Génomique Fonctionnelle, Montpellier, F-34094 France, [§]INSERM, U1191, Montpellier, F-34094 France, [¶]Plateforme de Vectorologie, Biocampus Montpellier CNRS UMS 3426, INSERM US009, Montpellier, F-34094 France, [‖]LabEx "Ion Channel Science and Therapeutics," Montpellier, F-34094 France, [**]Sorbonne Universités, Université Pierre et Marie Curie Université Paris 06, UM 119, Neuroscience Paris Seine (NPS), Paris F-75005, France, [‡‡]CNRS UMR 8246, NPS, Paris F-75005, France, and [§§]INSERM, U1130, NPS, Paris F-75005, France

Background: Novel strategies are needed to characterize the properties of T-type (Cav3) calcium channel isoforms.
Results: The I-II loop of the Cav3.2 protein potently inhibits both recombinant and neuronal Cav3.1 and Cav3.2 channels.
Conclusion: This I-II loop region can be used to selectively silence Cav3.1/Cav3.2 channels.
Significance: This study reveals a new approach to differentiate among the activity of native Cav3 channels.

Voltage-dependent calcium channels (Cav) of the T-type family (Cav3.1, Cav3.2, and Cav3.3) are activated by low threshold membrane depolarization and contribute greatly to neuronal network excitability. Enhanced T-type channel activity, especially Cav3.2, contributes to disease states, including absence epilepsy. Interestingly, the intracellular loop connecting domains I and II (I-II loop) of Cav3.2 channels is implicated in the control of both surface expression and channel gating, indicating that this I-II loop plays an important regulatory role in T-type current. Here we describe that co-expression of this I-II loop or its proximal region (Δ1-Cav3.2; Ser^{423}–Pro^{542}) together with recombinant full-length Cav3.2 channel inhibited T-type current without affecting channel expression and membrane incorporation. Similar T-type current inhibition was obtained in NG 108-15 neuroblastoma cells that constitutively express Cav3.2 channels. Of interest, Δ1-Cav3.2 inhibited both Cav3.2 and Cav3.1 but not Cav3.3 currents. Efficacy of Δ1-Cav3.2 to inhibit native T-type channels was assessed in thalamic neurons using viral transduction. We describe that T-type current was significantly inhibited in the ventrobasal neurons that express Cav3.1, whereas in *nucleus reticularis thalami* neurons that express Cav3.2 and Cav3.3 channels, only the fast inactivating T-type current (Cav3.2 component) was significantly inhibited. Altogether, these data describe a new strategy to differentially inhibit Cav3 isoforms of the T-type calcium channels.

T-type, low voltage-activated calcium channels are present in many excitable cells, especially in neurons, where they are critical to operate multiple physiological processes, including neuronal firing, neurotransmitter release, and slow wave sleep (1). In addition, substantial evidence supports a role of T-type calcium channels in diseases, especially in epilepsy and pain (2, 3). Indeed, enhanced activity of neuronal T-type channels would play a pathogenic role in the initiation of seizures and pain signal transmission (4).

Importantly, T-type calcium channels exhibit diversity in function and structure. They are encoded by three Cav3[2] subunits (Cav3.1, Cav3.2, and Cav3.3) (for a review, see Ref. 5). Functional expression studies have revealed that these Cav3 subunits all display low threshold activity. However, they markedly differ in some other electrophysiological properties. Strikingly, the Cav3.1 and Cav3.2 subunits are typical fast inactivating T-type channels, whereas the Cav3.3 subunit exhibits much slower activation and inactivation kinetics (6, 7).

Within the central nervous system, the Cav3.1, Cav3.2, and Cav3.3 subunits are differentially expressed in the various neuronal populations (8). However, the precise contributions of each of the three Cav3 subunits to neuron function remain elusive. This is well exemplified in the thalamus where the GABAergic neurons from the *nucleus reticularis thalami* (NRT) express both Cav3.2 and Cav3.3 subunits, whereas the glutamatergic thalamocortical relay neurons only express the Cav3.1 channels (8, 9). The development of knock-out/transgenic mice has been useful to identify the main roles of the Cav3 subunits (9–11). Unfortunately, no pharmacological tools are available to date to discriminate more precisely among the specific roles of the Cav3 subunits.

Toward this goal, we have hypothesized that selective modulation of the Cav3 subunits could be possibly achieved using alternative molecular strategies. Recent studies have identified that the intracellular loop connecting domains I and II (I-II loop) of the Cav3.2 subunit plays an important role in control-

* This work was supported by Agence N*ationale de la Recherche Grants* ANR-10-BLAN-1601 (to P. L.) and ANR-09-MNPS-035 grants (to P. L., R. C. L., and N. L.). The authors declare that they have no conflicts of interest with the contents of this article.
[1] To whom correspondence should be addressed: Inst. de Génomique Fonctionnelle, 141 rue de la Cardonille, 34094 Montpellier Cedex 5, France. Tel.: 33-434-359-251; Fax: 33-467-542-432; E-mail: philippe.lory@igf.cnrs.fr.

[2] The abbreviations used are: Cav, voltage-dependent calcium channel; I-II loop, intracellular loop connecting domains I and II; VB, ventrobasal complex; NRT, *nucleus reticularis thalami*; TEA, tetraethylammonium; *I*, current; *V*, voltage; Nter, N-terminal region; D, domain; L, loop; Ctrl, control; Ω, ohms; LTS, low threshold calcium spike.

ling both expression at the plasma membrane and gating of the channel. The proximal part of this I-II loop (subsequent to domain I) was described as a "gating brake" (12). Interestingly, this I-II loop plays distinct roles in plasma membrane expression among the Cav3 channel family (13–15) with a major inhibitory role for Cav3.2, modest inhibitory role in Cav3.1, and forward trafficking role in Cav3.3 channels. Building on these early findings, we show in the present study using two heterologous expression systems, cell lines and thalamic slices, that the proximal I-II loop region of the Cav3.2 subunit can be designed as a molecular tool to specifically inhibit Cav3.1 and Cav3.2 currents without affecting Cav3.3 channel activity.

Experimental Procedures

Constructs—The cDNAs encoding the Cav3.1, Cav3.2, and Cav3.3 subunits were described earlier (7) as well as epitope-tagged Cav3 subunits (15, 16). The various truncated forms of Cav3.2 as well as the I-II loop fragments were generated using PCR techniques, cloned into pEGFP-C1 expression vector (BD Biosciences), and verified using automated DNA sequencing.

Cell Lines—Human embryonic kidney (HEK)-293 and rat neuroblastoma NG 108-15 cells were cultured as described previously (7, 15). Cells were plated at 50–70% confluence for optimal transfection using the JetPEI transfection reagent according to the manufacturer's protocol (QBiogene, Irvine, CA). The Cav1.2 construct was cotransfected with $\alpha 2/\delta 1$ and $\beta 1$b subunits (1:2:2 molar ratio) as described earlier (17). In all conditions, corresponding empty plasmids were used to adjust the quantity of the transfected material.

Subcloning and Virus Production—Δ1-Cav3.2 and Nter-Cav3.2 were subcloned into the Sindbis viral vector SINrep-(nsP2S^{726}) kindly provided by H. Marie (Institut de Pharmacologie Moléculaire et Cellulaire-CNRS UMR 7275). Recombinant SINrep(nsP2S^{726}) constructs and helper plasmid DH-BB(tRNA/TE12) (18) were transcribed *in vitro* into capped RNA using the Megascript SP6 kit (Ambion). Baby hamster kidney-21 (ATCC CCL-10) cells were electroporated with Δ1-Cav3.2 or Nter-Cav3.2 RNA and the helper RNA (20×10^6 cells/ml, 950 microfarads, 230 V) and grown for 24 h at 37 °C at 5% CO_2 in DMEM containing 5% fetal calf serum before collecting the cell supernatant containing viruses. The virus titer (3×10^9 infectious particles/ml) was determined after counting fluorescent baby hamster kidney-21 cells infected using a serial dilution of the virus stock.

Preparation and Infection of Brain Slices—All procedures involving experimental animals were carried out in accordance with the European Union Council Directive 86-609 and local ethics committee guidelines. All efforts were made to minimize animal suffering and the number of animals used. Brains were excised from 8–12-day-old Wistar rats. A block of tissue containing the thalamus was removed, placed in a cold (<4 °C) oxygenated (95% O_2 and 5% CO_2) solution of artificial cerebrospinal fluid (125 mM NaCl, 2.5 mM KCl, 0.4 mM $CaCl_2$, 1 mM $MgCl_2$, 1.25 mM NaH_2PO_4, 26 mM $NaHCO_3$, 25 mM glucose, 5 mM sodium pyruvate, and 1 mM kynurenic acid (pH 7.3, osmolarity 310 mOsM)). The block of tissue was glued, ventral surface uppermost, to the stage of a Vibroslice (Leica VT1000S), and 280–300-μm-thick horizontal slices containing the ventrobasal complex (VB) and the NRT were prepared using the internal capsule and the medial lemniscus as landmarks.

Slices (three to four per hemisphere) were stored for 30 min in an oxygenated incubation chamber containing artificial cerebrospinal fluid of the above composition and then transferred onto a Millicell CM membrane (Millipore) pre-equilibrated with culture medium (50% minimum Eagle's medium, 50% Hanks' balanced salt solution, 5.5 g/liter glucose, and 1 ml/liter penicillin-streptomycin; Invitrogen).

A 2-μl drop of the viral solution (titrated at 3×10^9 infectious particles/ml) was added in the thalamic area containing the VB and NRT. The slices were incubated overnight at 35 °C at 5% CO_2. Slices were then transferred in an incubating chamber and equilibrated in continuously oxygenated (95% O_2 and 5% CO_2) artificial cerebrospinal fluid of the above composition but without kynurenic acid and with 2 mM $CaCl_2$ for at least 1 h at room temperature before being transferred to the recording chamber.

Patch Clamp Recordings on Cultured Cells—In HEK-293 and NG 108-15 cells, T-type whole-cell patch clamp recordings were performed 2–3 days after transfection as described earlier (7). T-type currents were recorded using 2 mM Ca^{2+} at room temperature using a test pulse to −30 mV from a holding potential at −100 mV or a ramp stimulus protocol ranging from −100 to +100 mV over 200 ms. The current density was calculated according to the capacitance of the cell and expressed in pA/picofarad. Extracellular solution contained 2 mM $CaCl_2$, 160 mM TEACl, and 10 mM HEPES (pH 7.4 with TEAOH). Pipettes (2–3 MΩ) were filled with a solution containing 110 mM CsCl, 10 mM EGTA, 10 mM HEPES, 3 mM Mg-ATP, and 0.6 mM GTP (pH 7.2 with CsOH). Detailed acquisition and analysis procedures can be found elsewhere (7).

Patch Clamp Recordings on Slices—Slices were perfused (2.5 ml/min) continuously with oxygenated artificial cerebrospinal fluid recording solution containing 2 mM Ca^{2+} at room temperature. Using the patch clamp technique (Axopatch 200B amplifier, Clampex 10, Molecular Devices), whole-cell recordings in current or voltage clamp mode were performed in VB and NRT neurons visualized with an Olympus BX51WI (×60 lens). Infected neurons were identified on the basis of their GFP fluorescence. Recordings were filtered by a four-pole Bessel filter set at a corner frequency of 2 kHz, digitalized at 10 kHz, and later analyzed using Clampfit10 (Molecular Devices) and Igor 6 (Wavemetrics). For current clamp recordings, the electrodes (borosilicate glass capillaries; World Precision Instruments) were filled with the following solution: 140 mM K-$MeSO_4$, 0.1 mM $CaCl_2$, 5 mM $MgCl_2$, 1 mM EGTA, 10 mM HEPES, 4 mM Na-ATP, 15 mM phosphocreatine, and 50 units/ml creatine phosphokinase (pH 7.3, osmolarity 290 mOsM). For voltage clamp recording electrodes were filled with 110 mM CsCl, 10 mM HEPES, 10 mM EGTA, 5 mM $MgCl_2$, 4 mM Na-ATP, 0.6 mM Na-GTP, 15 mM phosphocreatine, and 150 units/ml creatine phosphokinase (pH 7.3 with CsOH, osmolarity 280 mOsM) (tip resistances, 1.5–2.2 MΩ; access resistance, <5 MΩ). At least 80% of the cell capacitance and series resistance were compensated. To isolate Ca^{2+} currents, the following were added to the extracellular solution: 10 mM TEACl (Sigma), 1 mM 4-aminopyridine (Sigma), 0.5 μM tetrodotoxin (Tocris), and 2 mM

CsCl (Sigma). Glutamatergic (50 μM DL-2-amino-5-phosphonovaleric acid and 10 μM 6-cyano-7-nitroquinoxaline-2,3-dione) and GABAergic (3 μM SR-95531) receptor antagonists (Tocris) were added to the perfusion medium to block the spontaneous synaptic activities.

Leak currents were subtracted off line using templates constructed from the current induced by a 10-mV hyperpolarizing step applied from −100 mV at the end of each recording. Activation current-voltage (*I-V*) curves were constructed from the currents obtained by successive depolarization steps ranging from −80 to −40 mV with 2.5-mV increments preceded by a 1-s-long hyperpolarizing period to −100 mV. Each curve was fitted with a modified Boltzmann equation: $I_{max} = G(V + 30)/[1 + \exp((V_{1/2} - V)/k)]$ where G is maximal conductance, V is membrane potential, $V_{1/2}$ is potential of half-activation, and k is the slope. Steady-state *I-V* curves were constructed from the maximal current amplitude evoked at −50 mV following a 1-s-long hyperpolarization ranging from −110 to −60 mV with 5-mV increments. Curves were fitted with a modified Boltzmann equation: $I/I_{max} = 1/[1 + \exp((V - V_{1/2})/k)]$.

Biochemistry—Surface expression measurement was performed using luminometry-ELISA analysis as described previously (15, 19). Briefly, 40 h following transfection, cells were fixed for 5 min in 4% paraformaldehyde followed by two washes in PBS. The surface expression was measured in non-permeabilized cells, and total expression was measured after Triton X-100 (0.1%) permeabilization. The expression of HA-tagged channels was measured using rat anti-HA (3F10, Roche Applied Science; 1:1000) and secondary goat anti-rat antibody coupled to horseradish peroxidase (1:5000). After extensive washes in PBS, SuperSignal substrate (Femto, Pierce) was added, and luminescence was measured (Victor 2 luminometer). The percentage of surface expression corresponds to the ratio of surface/total relative light unit values.

Western blotting and immunoprecipitation experiments were performed as described previously (19). Briefly, 48 h after transfection, HEK-293 cells were lysed with Nonidet P-40 buffer and a mixture of protease inhibitors (Roche Applied Science), and lysates were spun at 10,000 × *g* for 30 min at 4 °C. Protein content of the supernatant was determined using the BCA Protein Assay kit (Pierce), and 60 μg of proteins was loaded for SDS-PAGE. Proteins were then transferred onto nitrocellulose membranes and blocked with 5% powdered non-fat milk. Primary antibodies used to detect HA-tagged Cav3.2 protein (the rat 3F10 monoclonal antibody or anti-Cav3.2 (sc-16263, Santa Cruz Biotechnology)) or the GFP constructs (rabbit anti-enhanced GFP, Cliniscience) were incubated for 1 h at room temperature in PBS and 0.05% Tween buffer. After two washes, secondary HRP-coupled antibodies were incubated for 1 h in PBS and 0.05% Tween buffer. The signal was detected using the SuperSignal West Pico Chemiluminescent system (Pierce). For immunoprecipitation, cells were lysed in Nonidet P-40 buffer and a mixture of protease inhibitors supplemented with 10 mM *N*-ethylmaleimide for 30 min on ice. Clarified cell lysates were then incubated with anti-HA- or anti-GFP-conjugated magnetic beads (Sigma) or anti-enhanced GFP antibodies for 4 h at 4 °C. The beads were washed four times with lysis buffer and resuspended in 4× loading buffer, and the immunoprecipitates were then analyzed by SDS-PAGE and Western blotting.

Statistical Analysis—Data are presented as mean ± S.E. The *n* values indicated in the *histogram bars* indicate the number of recorded cells. Statistical significance was determined using either Student's unpaired *t* test or one-way analysis of variance with Dunnett's correction for multiple comparisons with * indicating $p < 0.05$, ** indicating $p < 0.01$, and *** indicating $p < 0.001$.

Results

Whole cell patch clamp recordings using heterologous expression of the full-length wild-type Cav3.2 channel in HEK-293 cells was used to identify regions of the Cav3.2 protein able to modulate Cav3.2 channel activity. In a previous study (19), we had described that co-expression of a truncated form of the Cav3.2 channel protein comprising domains I and II produced a dominant-negative effect on the wild-type Cav3.2 channels, leading to degradation of the full-length Cav3.2 protein and silencing of the corresponding T-type current. Fig. 1*A* shows that silencing of the Cav3.2 current was obtained with truncated Cav3.2 proteins that contain domain I (D1), domain II (D2), or the I-II loop (L12). The latter is responsible for a ~5-fold decrease in T-type current density ($n = 30$, $p < 0.001$; Fig. 1*A*). On the contrary, no change in T-type current density was observed when the full-length Cav3.2 channels were coexpressed with the domain III-IV distal part of the protein (D34) or with the N-terminal region (Nter), the loop between domains II and III (L23), the loop between domains III and IV (L34), and the C-terminal region ($p > 0.05$; Fig. 1*A*). Significant inhibition of the Cav3.2 T-type current was obtained with various L12 constructs (375-amino acid, GFP fusion, and internal ribosome entry site GFP constructs) as well as with shorter fragments of the I-II loop (Fig. 1*B*) designed as illustrated in Fig. 2*A*. Indeed, significant T-type current inhibition was obtained with a construct containing the first 119 amino acids, named Δ1 (Ser^{423}–Pro^{542}), enabling us to identify a given domain involved in this L12 inhibition of Cav3.2 T-type current. Importantly, inhibition of the current amplitude was not accompanied with a change in kinetics (Fig. 2*B*) or in the current-voltage relationship recorded using a ramp protocol (Fig. 2*C*) of the remaining Cav3.2 current.

Using a full-length Cav3.2 channel HA-tagged construct (Fig. 3*A* and Refs. 15 and 16), we performed luminometry experiments to evaluate the level of Cav3.2 protein at the plasma membrane when coexpressed with constructs inhibiting (L12) or not (Nter) Cav3.2 current. As reported previously, ~15% of the total HA-tagged Cav3.2 protein is present at the cell surface (see Ref. 15), and no change in surface expression of the HA-tagged Cav3.2 protein could be observed when coexpressed with either L12 or Nter GFP-fused construct (Fig. 3, *A* and *B*). To identify any change in the total amount of Cav3.2 protein, Western blotting was performed (Fig. 3, *C* and *D*). These experiments revealed that a similar amount of Cav3.2 protein was detected in the presence of GFP-L12 construct compared with GFP alone (Fig. 3*C*) and similarly when the experiments were conducted with the GFP-Nter construct (Fig. 3*D*).

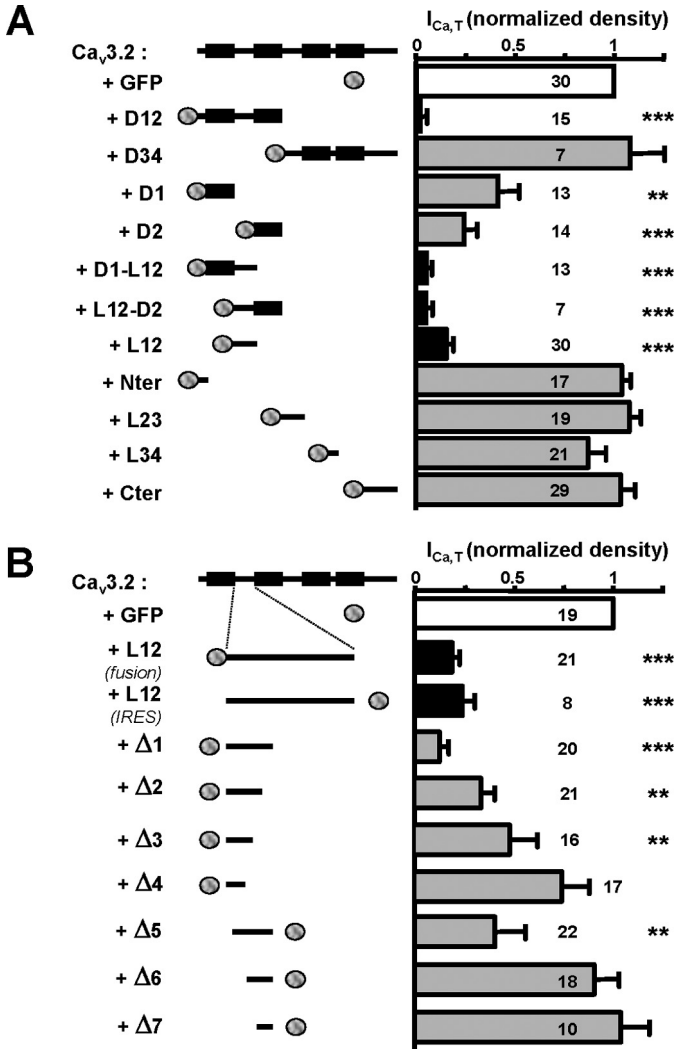

FIGURE 1. **T-type current inhibition obtained with various truncated forms of the Cav3.2 protein coexpressed with Cav3.2 channel.** *A*, normalized T-type current density recorded in HEK-293 cells expressing Cav3.2 channel in the presence of GFP alone or GFP-fused truncated forms of the Cav3.2 channel protein. The schematic structure of the Cav3.2 constructs is presented in the *left* part of the figure. *B*, normalized T-type current density in cells expressing Cav3.2 channel in the presence of various truncated forms of the I-II loop of Cav3.2 channel protein (Δ1–Δ7 constructs; see Fig. 2*A* for their amino acid sequences). For these constructs, the normalized residual Cav3.2 current densities ($I_{Ca,T}/I_{Ca,T\text{-}Ctrl}$) were as follows: Δ1, 0.12 ± 0.05, $n = 20$, $p < 0.001$; Δ2, 0.32 ± 0.07, $n = 21$, $p < 0.01$; Δ3, 0.47 ± 0.14, $n = 16$, $p < 0.01$; Δ4, 0.72 ± 0.14, $n = 17$, $p > 0.05$; Δ5, 0.39 ± 0.17, $n = 22$, $p < 0.001$; Δ6, 0.91 ± 0.13, $n = 20$, $p > 0.05$; Δ7, 1.04 ± 0.15, $n = 20$, $p > 0.05$. Note that coexpression of the I-II loop produces similar Cav3.2 current inhibition using either fusion ($I_{Ca,T}/I_{Ca,T\text{-}Ctrl} = 0.18 \pm 0.04$, $n = 21$, $p < 0.001$) or internal ribosome entry site (*IRES*) ($I_{Ca,T}/I_{Ca,T\text{-}Ctrl} = 0.25 \pm 0.08$, $n = 8$, $p < 0.001$) GFP constructs. Statistical significance was determined using one-way analysis of variance with Dunnett's correction for multiple comparisons (**, $p < 0.01$; ***, $p < 0.001$). *Error bars* represent S.E. *Cter*, C-terminal region.

Whether the I-II loop could interact with the full-length Cav3.2 protein was further investigated using co-immunoprecipitation experiments (Fig. 3, *E* and *F*). When the HA-tagged Cav3.2 protein was coexpressed with the GFP-L12 construct, the presence of the latter was detected following immunoprecipitation of the HA-tagged Cav3.2 protein (Fig. 3*E*, *arrow*), indicating that the I-II loop can form a protein complex with the full-length Cav3.2 protein. On the contrary, no such protein interaction could be detected when the HA-Cav3.2 protein was coexpressed with the GFP-Nter construct (Fig. 3*F*).

Considering that the I-II loop sequence of the Cav3.2 protein shares some similarities with other T-type/Cav3 channels, we also investigated its ability to inhibit Cav3.1 or Cav3.3 currents. When recombinant Cav3.1 channels were coexpressed together with the Δ1-Cav3.2 construct in HEK-293 cells, the T-type current density was reduced by ~3.2-fold ($n = 11$, $p < 0.01$; Fig. 4*A*). On the contrary, when this Δ1-Cav3.2 construct was coexpressed with Cav3.3 channels, no change in the current density could be observed ($n = 14$, $p > 0.05$; Fig. 4*B*). These data indicate that the Δ1 construct made of Cav3.2 protein could target both Cav3.2 and Cav3.1 channels but not Cav3.3 channels. In addition, coexpression of the Δ1-Cav3.2 construct with the L-type Cav1.2 channels (in the presence of auxiliary $\alpha 2\delta 1$ and $\beta 3$ subunits), resulted in no change in L-type current density ($n = 10$, $p > 0.05$; Fig. 4*C*). Similarly, no alteration of the P/Q-type current density (Cav2.1 in the presence of $\alpha 2\delta 1$ and $\beta 3$) was observed in the presence of the Δ1-Cav3.2 construct (not shown).

We next explored the ability of the I-II loop constructs (L12 and Δ1) to inhibit native Cav3.2 T-type current in the neuroblastoma cell line NG 108-15 (Fig. 5). Representative T-type currents traces obtained in the control condition (+GFP) and in the presence of L12 or Δ1 construct are shown in Fig. 5*A*. Significant inhibition (>10-fold) of the native T-type current density was obtained with the L12 and Δ1 constructs ($n = 15$ and $n = 10$, respectively; Fig. 5, *A* and *B*), demonstrating the efficacy of these I-II loop constructs to silence native Cav3.2 channels. Taking advantage of the presence of native Cav3.2 channels in NG 108-15 cells to further validate the specificity of I-II loop inhibition, we next investigated the inhibitory effect of the Cav3.1, Cav3.2, and Cav3.3 I-II loop constructs on NG 108-15 T-type currents (Fig. 5*C*). Importantly, the Cav3.1 I-II loop could silence native Cav3.2 T-type current in NG 108-15 cells (>20-fold, $n = 9$), but the Cav3.3 I-II loop could not ($n = 8$). These data demonstrate that I-II loop constructs (L12 and Δ1) made either of Cav3.1 or Cav3.2 proteins selectively target and silence Cav3.1 and Cav3.2 T-type channels. To further validate these data obtained using transient transfection procedures in NG 108-15, we developed a secondary NG 108-15 cell line expressing the Cav3.2 L12 in which the permanent expression of this L12 construct completely abolished the presence of the T-type current (not shown). Altogether, these data demonstrate that expression of the L12 or Δ1 construct of the Cav3.2 protein efficiently eliminates the presence of T-type currents in cells expressing Cav3.1 or Cav3.2 channels.

Next, we assessed the ability of the Δ1 fragment to suppress native T-type currents in thalamic neurons. The thalamus is one of the brain areas showing the strongest expression of Cav3 channels with thalamocortical neurons expressing the Cav3.1 T-type channel isoform, whereas the GABAergic neurons of the NRT express both Cav3.2 and Cav3.3 isoforms (8, 20). In both neuronal types, an accurate biophysical characterization of the T-type current can only be performed in young pups (P8–P12) due to the development profile of the T-type currents and space-clamp limitations. To meet this temporal

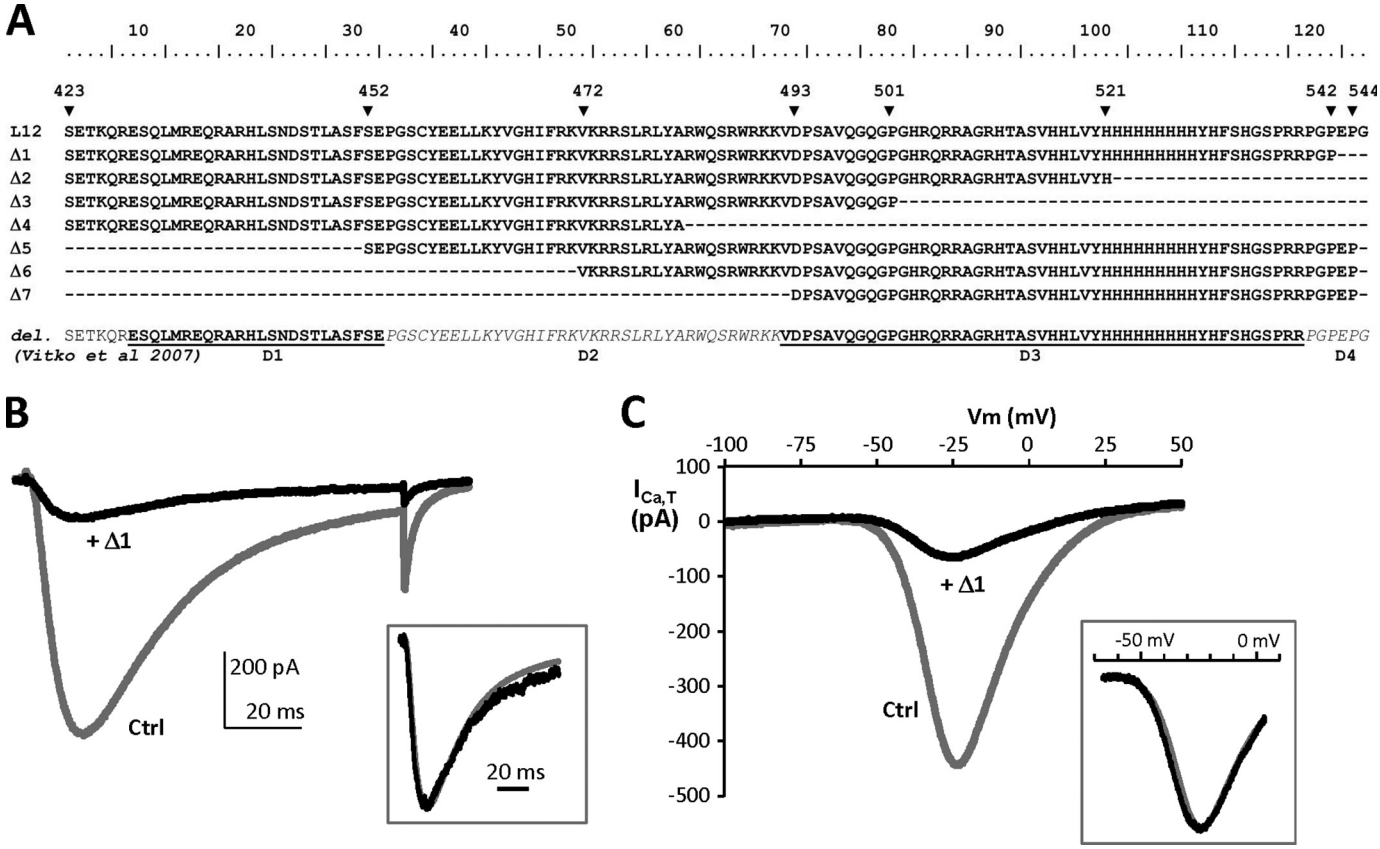

FIGURE 2. **Design of short (Δ) I-II loop constructs and representative electrophysiological properties of the Δ1 construct.** *A*, the amino acid sequences of the Δ1–Δ7 constructs were identified according to the human Cav3.2 protein entry in the UniProt database (O95180): Δ1 (Ser^{423}–Pro^{542}), Δ2 (Ser^{423}–His^{521}), Δ3 (Ser^{423}–Pro^{501}), Δ4 (Ser^{423}–Ala^{481}), Δ5 (Ser^{452}–Pro^{544}), Δ6 (Val^{472}–Pro^{544}), and Δ7 (Asp^{493}–Pro^{544}). These constructs are compared in this multiple alignment with the Cav3.2 deletion mutants (D1–D4) used in Vitko *et al.* (15). *B*, superimposed representative T-type current traces recorded using a test pulse at −30 mV from a holding potential of −100 mV (100-ms duration) on HEK-293 cells transfected with Cav3.2 and Nter constructs (Ctrl; *gray* trace) and Cav3.2 and Δ1 constructs (+Δ1; *black* trace). The traces were normalized in amplitude (*inset*), which revealed no difference in the activation and inactivation kinetics of the residual Cav3.2 current in cells expressing the Δ1 construct. *C*, representative T-type currents recorded using a ramp test (−100/+100 mV; holding potential, −100 mV; 200-ms duration) on HEK-293 cells transfected with Cav3.2 and Nter constructs (Ctrl; *gray* trace) and Cav3.2 and Δ1 constructs (+Δ1; *black* trace). Traces were normalized in amplitude (*inset*), revealing no shift in the current-voltage relationship of the residual Cav3.2 current in cells expressing the Δ1 construct.

constraint, we selected a fast expressing system using Sindbis viral constructs.

Freshly prepared thalamic slices were infected with either a GFP-Δ1-expressing virus (Δ1) or a control GFP-Nter-expressing virus (Ctrl), and whole-cell recordings of neurons located in the VB and NRT were performed 12–24 h after infection (see "Experimental Procedures"). Current clamp recordings showed that thalamocortical Δ1-infected neurons, GFP-Nter-expressing neurons (Ctrl) and non-fluorescent (*i.e.* non-transfected) neurons displayed similar input resistances (Ctrl, 314.3 ± 59.8 MΩ, $n = 12$; Δ1, 388.8 ± 47.5 MΩ, $n = 12$; non-transfected, 353.6 ± 63.6 MΩ, $n = 7$; $p > 0.5$) and resting membrane potentials (Ctrl:, −73.7 ± 1.7 mV, $n = 12$; Δ1, −68.5 ± 2.1 mV, $n = 12$; non-transfected, −71.9 ± 1.8 mV, $n = 7$; $p > 0.5$). However, the maximal firing rates evoked during depolarizing current injections were identical in Δ1 and control neurons (Ctrl, 19.5 ± 1.3 Hz, $n = 10$; Δ1, 22 ± 1.8 Hz, $n = 10$; $p = 0.27$) but significantly higher in non-transfected neurons (28.9 ± 1.3 Hz, $n = 7$; $p < 0.02$) indicating that the virus *per se* may change some active properties of the neurons.

Considering the voltage-gated calcium currents, VB Δ1-infected neurons showed a drastic decrease in the total T-type current evoked at −50 mV after a 1-s hyperpolarizing prepulse to −100 mV (Ctrl, 1425 ± 112 pA, $n = 18$; Δ1, 377 ± 37 pA, $n = 26$; $p < 0.001$; Fig. 6, *A* and *B*), whereas the amplitude of the currents recorded in control and in non-transfected neurons (1518 ± 120 pA, $n = 15$) were identical ($p = 0.6$). Inactivation decay was best fitted with a single time constant typical of Cav3.1 current of VB neurons (21), and no difference was observed between the Δ1 (τ, 13.7 ± 0.3 ms, $n = 18$) and control conditions (τ, 12.8 ± 1.6 ms, $n = 18$; $p = 0.065$; Fig. 6*C*). Activation and inactivation voltage dependences were similar in both conditions (activation $V_{1/2}$: Δ1, −60.0 ± 0.5 mV, $n = 8$ *versus* Ctrl, −61.4 ± 0.8 mV, $n = 8$; $p = 0.15$ and inactivation $V_{1/2}$: Δ1, −86.3 ± 1.5 mV, $n = 8$ *versus* Ctrl, −86.2 ± 1.1 mV, $n = 10$; $p = 0.95$). Importantly, the amplitude of the high voltage-activated current evoked by a step depolarization from −60 to +10 mV was unchanged for Δ1-infected and control neurons (2700.5 ± 284 pA ($n = 12$) and 2864 ± 259 pA ($n = 11$, respectively; $p = 0.67$).

In NRT neurons infected by the control GFP-Nter-expressing virus, the inactivation decay of T-type current was described by a double exponential function with the fast (τ1, 16.4 ± 1.0 ms) and slow (τ2, 82 ± 3.0 ms; $n = 10$) components

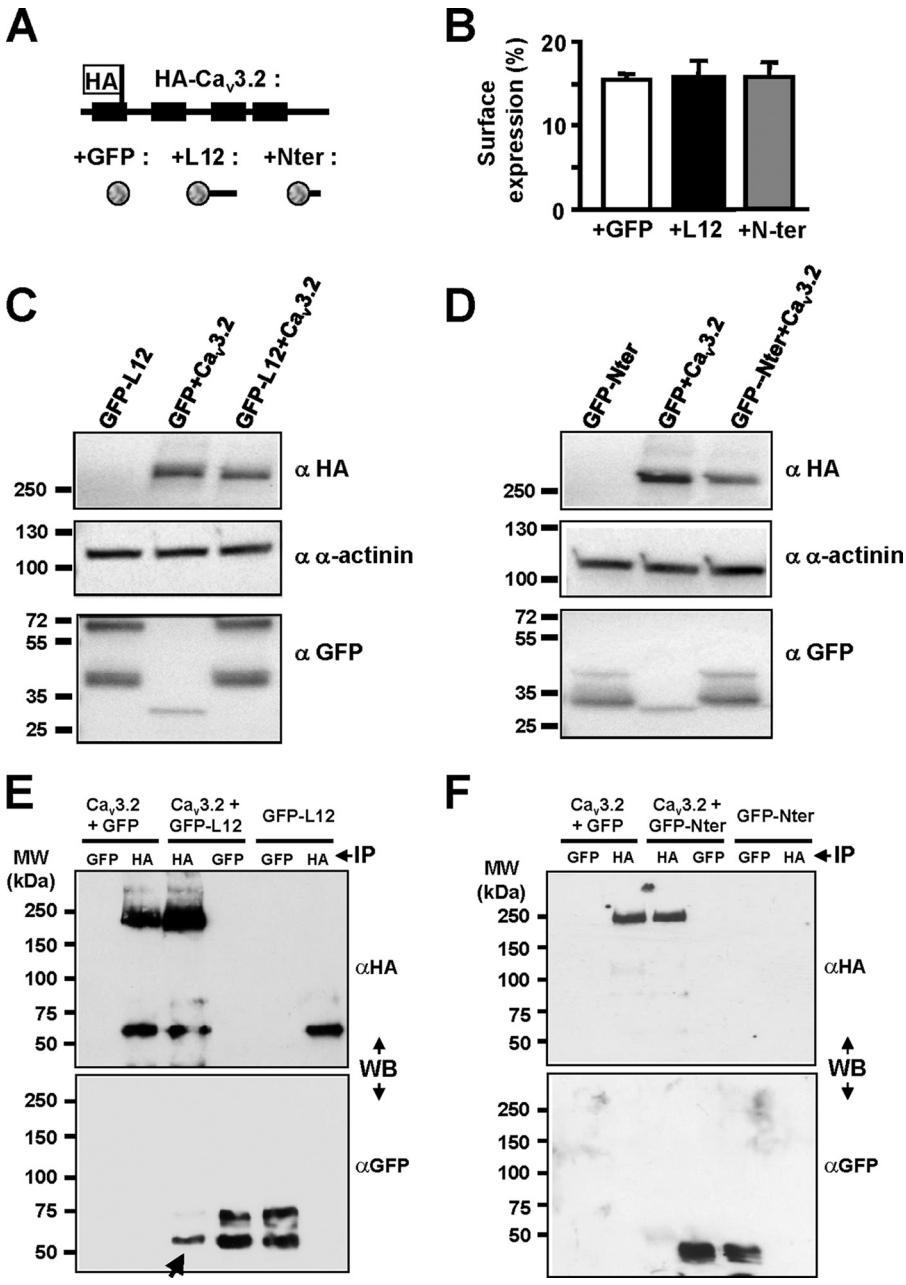

FIGURE 3. **Biochemical properties of the Cav3.2 channel when coexpressed with I-II loop construct.** *A* and *B*, luminometry detection of the surface expression of the HA-Cav3.2 construct (schematic structure presented in *A*) in the presence of free GFP (*B*, *white bar*), GFP-tagged I-II loop (*B*, *black bar*), and GFP-tagged Nter constructs (*B*, *gray bar*). *C*, Western blot analysis of the total HA-Cav3.2 protein amount in cells co-transfected with I-II loop (*right lane*) compared with the total amount of Cav3.2 protein in cells co-transfected with GFP (*middle lane*). *D*, Western blotting (*WB*) experiments similar to those in *C* performed in the presence of the Nter construct. *E* and *F*, co-immunoprecipitation (*IP*) experiments for the transfection conditions indicated at the *top* of the figure showing that the I-II loop protein could be detected (*E*, *arrow*) when the HA-Cav3.2 protein was immunoprecipitated but not when the HA-Cav3.2 protein was coexpressed with the Nter (*F*). *Error bars* represent S.E.

reflecting the presence of the Cav3.2 and Cav3.3 channels, respectively. Similarly to VB neurons, all NRT Δ1-infected neurons showed a significant decrease in the total T-type current (Ctrl; 1048 ± 122 pA; $n = 10$; Δ1; 537 ± 57 pA, $n = 9$; $p < 0.001$; Fig. 6, *D* and *E*). In three of the nine Δ1-infected NRT neurons, the inactivation decay was fitted by a single exponential function with a time constant of 61.7 ± 8.5 ms, which is similar to the slow time constant ($\tau 2$) of the control T-type current (Fig. 6*F*). In the six remaining Δ1-infected neurons, the decay of the T-type current was still described by a double exponential function with time constants similar to those of the control current. Of importance, the weight of the fast time constant was markedly reduced (Δ1, 267 ± 27 pA; Ctrl, 685 ± 217 pA; $p < 0.01$), whereas the weight of the slow time constant was unchanged (Δ1, 304 ± 19 pA; Ctrl, 300 ± 36 pA; $p = 0.94$). Hence, in all Δ1-infected NRT neurons, the fast component of the T-type current presumably due to the Cav3.2 channels was almost fully blocked. Altogether, these data confirm the results obtained in the recombinant system showing that only the fast inactivating Cav3.1 and Cav3.2 currents are inhibited in the presence of the Δ1 construct, whereas Cav3.3 and high voltage-activated currents are unchanged.

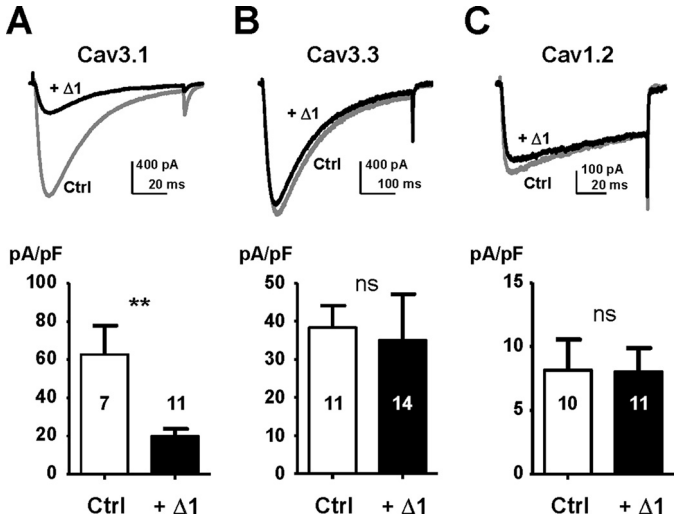

FIGURE 4. **No Cav3.3 current and Cav1.2 current inhibition in the presence of the I-II loop construct.** The effect of the shorter I-II loop construct Δ1 on other Cav channels is shown. There was an inhibitory effect of the Δ1 construct on Cav3.1 current (*A*) but not on Cav3.3 current (*B*) and Cav1.2 current (*C*). Representative current traces are presented in the *top* part of the panels (Ctrl and +Δ1), and the average current densities are shown in the *bottom* part of the panels. Statistical significance was determined using Student's unpaired *t* test (**, $p < 0.01$; *ns*, non-significant). *Error bars* represent S.E. *pF*, picofarad.

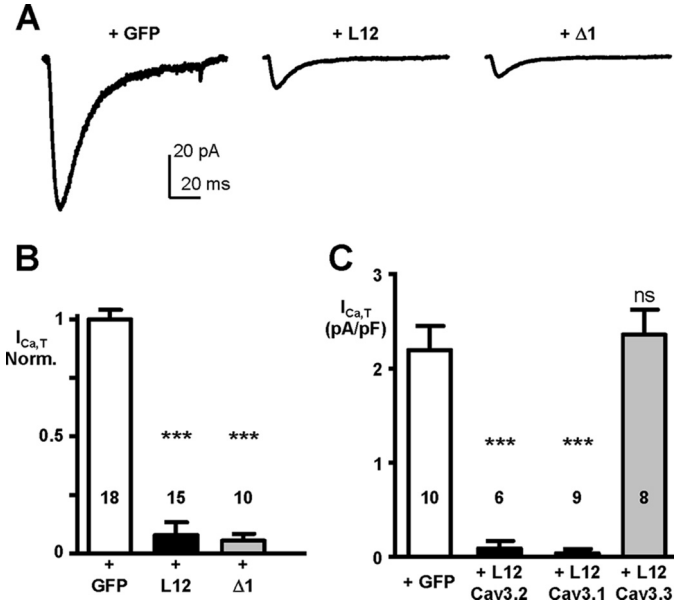

FIGURE 5. **Silencing effect of the I-II loop and Δ1 constructs on native T-type current (Cav3.2) channels in NG 108-15 cells.** *A*, examples of T-type current traces recorded in NG 108-15 cells (holding potential, −100 mV; test pulse, −30 mV) transfected with GFP (*left* part), with the I-II loop construct (L12; *middle* part), with the Δ1 construct (*right* part). *B*, average inhibitory effects of the Cav3.2 I-II loop and Δ1 constructs on native T-type current in NG 108-15 cells. *C*, efficacy of the I-II loop constructs generated from the Cav3.1, Cav3.2, and Cav3.3 channels on native T-type current in NG 108-15 cells. Note the absence of inhibitory effect of the I-II loop construct generated from the Cav3.3 channel. Statistical significance was determined using Student's unpaired *t* test (***, $p < 0.001$; *ns*, non-significant). *Error bars* represent S.E. *Norm.*, normalized.

Finally, to assess the effects of the Δ1-induced decrease in T-type current amplitude on neuronal excitability, we evoked a rebound low threshold calcium spike (LTS) in thalamocortical neurons. Following 1-s-long hyperpolarization to −100 mV that allows de-inactivation of the whole T-type channel population, rebound LTS crowned by at least one action potential was evoked in the 12 control neurons recorded (Fig. 6*G*, *left panel*) but failed to evoked an action potential in two of the 12 neurons expressing the Δ1 construct (Fig. 6*G*, *middle panel*). Considering that the Δ1 construct decreased by 74% the amplitude of the T-type current, this moderate failure rate in Δ1 neurons is in agreement with our previous data showing that more than 70% of the T-type channel population needs to be blocked to hamper the LTS-associated firing in thalamic neurons (22). Accordingly, when the hyperpolarizing potential was reduced to ~−85 mV, a value corresponding to the half-inactivation of the T-type current, LTS crowned by an action potential was still recorded in six of the 12 control neurons but only in three of the 12 Δ1-infected neurons (Fig. 6*G*, *right panel*).

Discussion

Here we document that overexpression of the I-II loop of the Cav3.2 subunit of T-type calcium channels induces silencing of the Cav3.1/Cav3.2 T-type currents without affecting Cav3 protein expression at the plasma membrane. This inhibitory effect on Cav3.1/Cav3.2 currents is produced by the proximal part of the I-II loop, and Cav3.2 currents were unchanged upon expression of the other intracellular regions of the Cav3.2 channel. This study reveals a novel aspect of T-type Cav3 channel regulation that involves its I-II loop and can be used to block selectively the activity of native Cav3.1/Cav3.2 channels, such as in neurons.

Importantly, we found that the amount of Cav3.2 protein as well as its expression at the plasma membrane was unchanged in the presence of the I-II loop. This finding indicates that the silencing effect produced by the I-II loop does not involve a retention/degradation mechanism of the wild-type Cav3.2 channel, which was observed with the truncated forms of Cav3.2 that include domain I and/or domain II (19). To characterize further the mechanism involved in the I-II loop silencing effect, we searched for the domain involved by using shorter fragments, but we were unsuccessful in identifying the specific protein domain(s) as truncated forms of the I-II loop shorter than the proximal ~100-amino acid-long peptide were less efficient in producing the inhibitory effect. The precise molecular mechanism supporting this silencing effect remains to be identified. However, several observations should be considered. (i) It likely involves molecular interactions as co-immunoprecipitation experiments have revealed association of the I-II loop with the full-length Cav3.2 protein. (ii) Stability and plasma membrane expression of Cav3.2 protein are not altered, indicating that Cav3.2 channels are correctly processed to the cell surface when the I-II loop is overexpressed. (iii) The remaining T-type calcium currents in cells overexpressing the I-II loop are unaffected in their kinetics and steady-state properties, suggesting an "all or none" silencing effect for channels associated with the I-II loop. To account for this silencing mechanism, we hypothesize that the Cav3.1/Cav3.2 channels are locked in a non-conducting closed state or inactivated state in the presence of a I-II loop overload. Our data are also well supportive of the previous description of a gating brake role of the I-II loop in Cav3.2 and to a lesser extent in Cav3.1 but not Cav3.3 channels (12, 13, 15). Altogether, this "dominant-negative'" strategy rep-

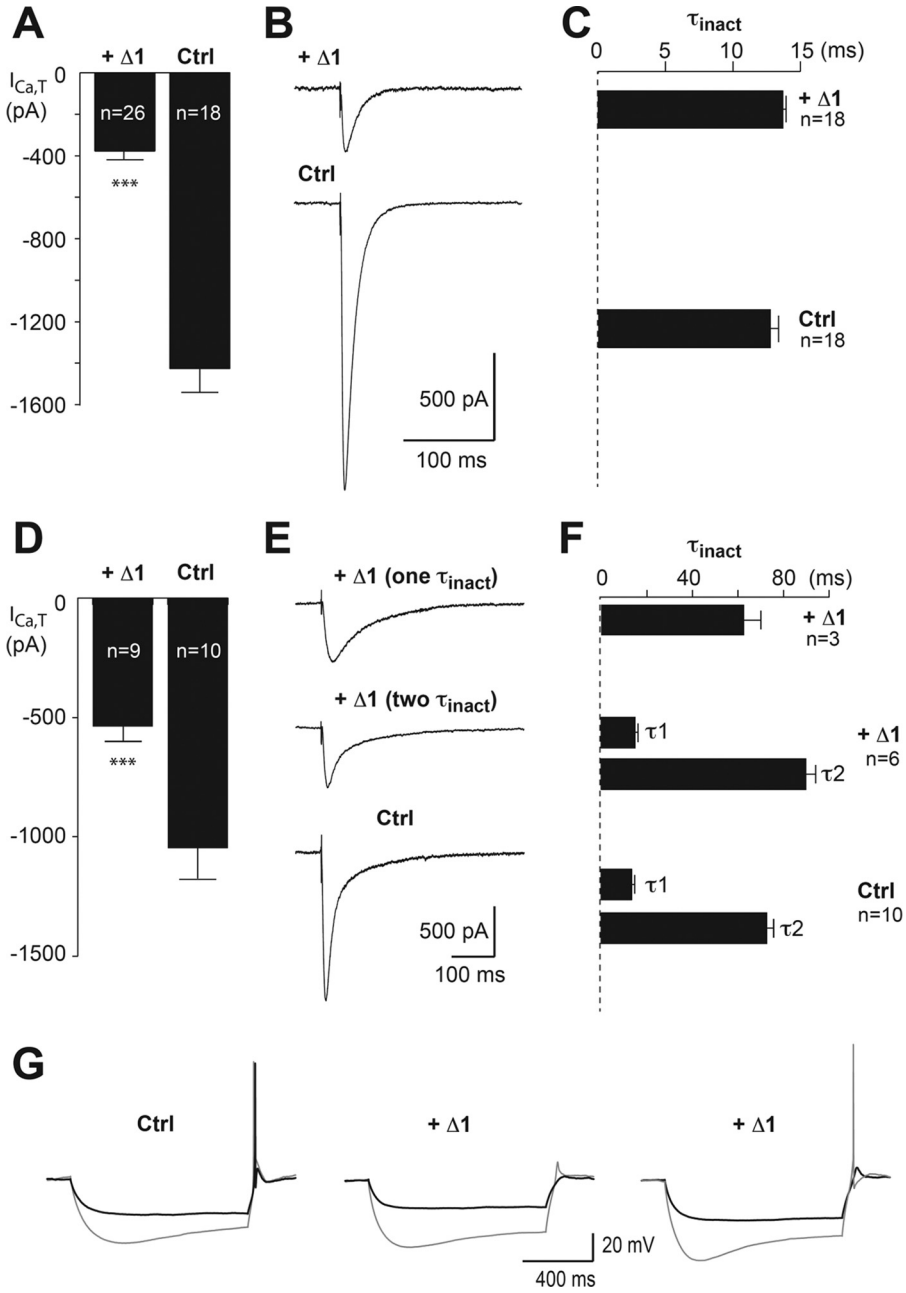

FIGURE 6. **Silencing effect of the Δ1 construct on thalamic T-type currents.** *A*, mean amplitude of T-type currents recorded in VB neurons infected with either the Δ1-expressing virus or the control GFP-Nter-expressing virus (Ctrl). T-type currents were evoked by step depolarization (200 ms long) to −50 mV after a 1-s hyperpolarizing prepulse to −100 mV. *B*, examples of T-type currents recorded in both conditions. *C*, mean values of the inactivation time constant. *D*, mean amplitude of T-type currents recorded in NRT neurons infected with either the Δ1-expressing virus or the control GFP-Nter-expressing virus (Ctrl). The protocol used was the same protocol as in A. *E*, examples of T-type currents recorded in both conditions. The *top* traces show T-type currents recorded in Δ1-infected neurons displaying an inactivation kinetic described with either one or two time constants. *F*, mean values of the inactivation time constants. Note that when the decay of the T-type current recorded in Δ1-infected neurons is described by a single time constant its value is identical to those of the slow time constant ($\tau 2$) of the T-type currents recorded in Δ1-infected and control neurons. Statistical significance was determined using Student's unpaired *t* test (***, $p < 0.001$). *G*, typical rebound LTS evoked by 1-s-long hyperpolarizing steps in control (*left* traces) and Δ1-infected (*middle* and *right* traces) thalamocortical neurons. Note that rebound LTS-associated firing was evoked following −100-mV hyperpolarizing steps in the 12 recorded control neurons (*left*, *gray* trace) and was still present after a −85-mV hyperpolarization in six neurons (*left*, *black* trace). When considering the Δ1-infected neurons, if a rebound firing was still observed following −100-mV hyperpolarizing steps in 10 of 12 neurons (*right versus middle*, *gray* traces), then reducing the hyperpolarizing potential to −85 mV suppressed LTS firing in nine of the 12 neurons (*middle* and *right*, *black* traces). *Error bars* represent S.E.

resents an original alternative to eliminate Cav3.1/Cav3.2 channels at the functional level without altering their protein expression.

Indeed, an important finding of our study is that delivery of the I-II loop into neurons could efficiently silence native Cav3.2 and Cav3.1 channels. Clear evidence was first obtained in the neuroblastoma cell line NG 108-15, which expresses T-type calcium channels made of Cav3.2 subunit (7). Both transient and stable expression of I-II loop constructs (L12 and Δ1) resulted in a complete disappearance of the T-type current in NG 108-15 cells. Importantly, similar findings were obtained in VB and NRT thalamic neurons following viral delivery of the Δ1

construct. In VB neurons that express the Cav3.1 isoform, the T-type current density was significantly reduced with no change in current properties, such as inactivation kinetics and activation and inactivation voltage dependences. In NRT neurons that express both the Cav3.2 and the Cav3.3 isoforms, the T-type current density was also significantly reduced. Inactivation kinetics analysis revealed that only the Cav3.2 fast inactivating component was eliminated, whereas the slow inactivating component attributable to Cav3.3 T-type current was unaffected. Altogether, these findings demonstrate that silencing of native Cav3.1/Cav3.2 channels can be achieved using delivery of I-II loop constructs. This strategy greatly expands the current means to investigate the role of the neuronal Cav3 channels as it allows manipulating the Cav3.1 and Cav3.2 subunit activities in a time- and region-selective manner even in chronically monitored animals without affecting the amount of Cav3 protein as observed in knock-out animals or using RNA interference strategies. In addition, its lack of effect on the Cav3.3 isoform will allow deciphering the respective role of fast and slow inactivating T-type currents in brain areas or neurons where both channels are expressed.

References

1. Lambert, R. C., Bessaïh, T., Crunelli, V., and Leresche, N. (2014) The many faces of T-type calcium channels. *Pflugers Arch.* **466,** 415–423
2. François, A., Laffray, S., Pizzoccaro, A., Eschalier, A., and Bourinet, E. (2014) T-type calcium channels in chronic pain: mouse models and specific blockers. *Pflugers Arch.* **466,** 707–717
3. Zamponi, G. W., Lory, P., and Perez-Reyes, E. (2010) Role of voltage-gated calcium channels in epilepsy. *Pflugers Arch.* **460,** 395–403
4. Cheong, E., and Shin, H. S. (2013) T-type Ca^{2+} channels in normal and abnormal brain functions. *Physiol. Rev.* **93,** 961–992
5. Perez-Reyes, E. (2003) Molecular physiology of low-voltage-activated T-type calcium channels. *Physiol. Rev.* **83,** 117–161
6. Cain, S. M., and Snutch, T. P. (2010) Contributions of T-type calcium channel isoforms to neuronal firing. *Channels* **4,** 475–482
7. Chemin, J., Monteil, A., Perez-Reyes, E., Bourinet, E., Nargeot, J., and Lory, P. (2002) Specific contribution of human T-type calcium channel isotypes (α_{1G}, α_{1H} and α_{1I}) to neuronal excitability. *J. Physiol.* **540,** 3–14
8. Talley, E. M., Cribbs, L. L., Lee, J. H., Daud, A., Perez-Reyes, E., and Bayliss, D. A. (1999) Differential distribution of three members of a gene family encoding low voltage-activated (T-type) calcium channels. *J. Neurosci.* **19,** 1895–1911
9. Kim, D., Song, I., Keum, S., Lee, T., Jeong, M. J., Kim, S. S., McEnery, M. W., and Shin, H. S. (2001) Lack of the burst firing of thalamocortical relay neurons and resistance to absence seizures in mice lacking α_{1G} T-type Ca^{2+} channels. *Neuron* **31,** 35–45
10. Astori, S., and Lüthi, A. (2013) Synaptic plasticity at intrathalamic connections via CaV3.3 T-type Ca^{2+} channels and GluN2B-containing NMDA receptors. *J. Neurosci.* **33,** 624–630
11. Ernst, W. L., Zhang, Y., Yoo, J. W., Ernst, S. J., and Noebels, J. L. (2009) Genetic enhancement of thalamocortical network activity by elevating alpha 1g-mediated low-voltage-activated calcium current induces pure absence epilepsy. *J. Neurosci.* **29,** 1615–1625
12. Arias-Olguín, I. I., Vitko, I., Fortuna, M., Baumgart, J. P., Sokolova, S., Shumilin, I. A., Van Deusen, A., Soriano-García, M., Gomora, J. C., and Perez-Reyes, E. (2008) Characterization of the gating brake in the I-II loop of $Ca_v3.2$ T-type Ca^{2+} channels. *J. Biol. Chem.* **283,** 8136–8144
13. Baumgart, J. P., Vitko, I., Bidaud, I., Kondratskyi, A., Lory, P., and Perez-Reyes, E. (2008) I-II loop structural determinants in the gating and surface expression of low voltage-activated calcium channels. *PLoS One* **3,** e2976
14. Shcheglovitov, A., Vitko, I., Bidaud, I., Baumgart, J. P., Navarro-Gonzalez, M. F., Grayson, T. H., Lory, P., Hill, C. E., and Perez-Reyes, E. (2008) Alternative splicing within the I-II loop controls surface expression of T-type $Ca_v3.1$ calcium channels. *FEBS Lett.* **582,** 3765–3770
15. Vitko, I., Bidaud, I., Arias, J. M., Mezghrani, A., Lory, P., and Perez-Reyes, E. (2007) The I-II loop controls plasma membrane expression and gating of $Ca_v3.2$ T-type Ca^{2+} channels: a paradigm for childhood absence epilepsy mutations. *J. Neurosci.* **27,** 322–330
16. Dubel, S. J., Altier, C., Chaumont, S., Lory, P., Bourinet, E., and Nargeot, J. (2004) Plasma membrane expression of T-type calcium channel α_1 subunits is modulated by high voltage-activated auxiliary subunits. *J. Biol. Chem.* **279,** 29263–29269
17. Bidaud, I., and Lory, P. (2011) Hallmarks of the channelopathies associated with L-type calcium channels: a focus on the Timothy mutations in $Ca_v1.2$ channels. *Biochimie* **93,** 2080–2086
18. Kim, J., Dittgen, T., Nimmerjahn, A., Waters, J., Pawlak, V., Helmchen, F., Schlesinger, S., Seeburg, P. H., and Osten, P. (2004) Sindbis vector SINrep(nsP2S726): a tool for rapid heterologous expression with attenuated cytotoxicity in neurons. *J. Neurosci. Methods* **133,** 81–90
19. Mezghrani, A., Monteil, A., Watschinger, K., Sinnegger-Brauns, M. J., Barrère, C., Bourinet, E., Nargeot, J., Striessnig, J., and Lory, P. (2008) A destructive interaction mechanism accounts for dominant-negative effects of misfolded mutants of voltage-gated calcium channels. *J. Neurosci.* **28,** 4501–4511
20. Huguenard, J. R., and Prince, D. A. (1992) A novel T-type current underlies prolonged Ca^{2+}-dependent burst firing in GABAergic neurons of rat thalamic reticular nucleus. *J. Neurosci.* **12,** 3804–3817
21. Leresche, N., Parri, H. R., Erdemli, G., Guyon, A., Turner, J. P., Williams, S. R., Asprodini, E., and Crunelli, V. (1998) On the action of the anti-absence drug ethosuximide in the rat and cat thalamus. *J. Neurosci.* **18,** 4842–4853
22. Dreyfus, F. M., Tscherter, A., Errington, A. C., Renger, J. J., Shin, H. S., Uebele, V. N., Crunelli, V., Lambert, R. C., and Leresche, N. (2010) Selective T-type calcium channel block in thalamic neurons reveals channel redundancy and physiological impact of $I_{Twindow}$. *J. Neurosci.* **30,** 99–109

Inhibition of Cav3.2 T-type Calcium Channels by Its Intracellular I-II Loop

Arnaud Monteil, Patrick Chausson, Katia Boutourlinsky, Alexandre Mezghrani, Sylvaine Huc-Brandt, Iulia Blesneac, Isabelle Bidaud, Céline Lemmers, Nathalie Leresche, Régis C. Lambert and Philippe Lory

J. Biol. Chem. 2015, 290:16168-16176.
doi: 10.1074/jbc.M114.634261 originally published online April 30, 2015
